Journal of Polymers and the Environment (2018) 26:4405–4414
https://doi.org/10.1007/s10924-018-1311-7

ORIGINAL PAPER

Fully Bio-Sourced Nylon 11/Raw Lignin Composites: Thermal and Mechanical Performances

N. Sallem-Idrissi[1] · P. Van Velthem[2] · M. Sclavons[2]

Published online: 25 September 2018

Abstract
Ecofriendly fully bio-composites based on polyamide 11 (PA11) and lignin have been prepared on the entire concentration range using a twin-screw extruder. In this work, PA11 was blended with lignin by direct extrusion technology without any chemical pre- or in-situ- modifications or physical pretreatments. The presence of various organic and inorganic impurities in the selected technical lignin have been maintained. The incorporation of this cheap renewable material from biomass in bio-based PA11 was inspected by an array of characterization tools. Also, the effect of the presence of lignin on the morphology and on the mechanical properties of the resulting materials was examined. Finally, in-situ investigation of structural evolution in PA11 induced by the presence of lignin was analyzed by Fast Scanning Chip Calorimetry.

Keywords Lignin · Polyamide 11 · Extrusion · Bio-sourced composite

Introduction

Nowadays, plastics obtained from renewable raw materials present one relevant solution for progressive replacement of fossil based polymers. In this request for sustainable development for these kinds of materials, green composites embedding natural fillers with renewable resourced-based biopolymers are gaining prominence todays. These materials have been selected due to a better environmental impact compared to conventional polymers as well as to endorse an improvement in their current properties. Moreover, the final composite specific performance properties could also be influenced by the additives such as plasticizers, heat and light stabilizers.

Among a variety of commercially available biopolymers, a group of agro-sourced polyamides has been introduced into the market. These bio-polyamides such as polyamide 11 (PA11) are usually obtained by the condensation reaction of diamines and dicarboxylic acids from castor oil and are depicted as an interesting alternative to their petroleum-based counterparts [1]. PA11 is a thermoplastic polymer with a low melting point compared to other polyamides (about 200 °C). This allows PA11 to be natural fillers reinforced with relatively low or even no thermal degradation at all of the natural fillers. Moreover, thanks to its non-biodegradability, high water and chemical resistance, PA11 offers a great potential to develop sophisticated and sustainable bio-composites for long-life applications [2].

In the group of natural polymers, lignin, one of the major components of wood along with cellulose and hemicellulose, is available in large quantities in paper plant and biorefineries, in which it is frequently used as a low-cost fuel for their internal energy needs [3–5]. Furthermore, lignin is also available in the agricultural non-food commercial plant as residues. Lignin could potentially be used for higher value-added applications. Considering its chemical composition, it would especially be appropriate as a source of raw, renewable and inexpensive materials for the plastic industries [6]. Lignin holds a number of advantages compared to synthetic materials such as being CO_2 neutral, biodegradable and as previously noted, abundantly available.

Unfortunately, various factors related to its structural characteristics in particular as an unsteady precursor to

✉ N. Sallem-Idrissi
naima.sallem@uclouvain.be

[1] Materials and Process Engineering (IMAP), Institute of Mechanics, Materials and Civil Engineering (iMMC), Université catholique de Louvain (UCL), Place Sainte Barbe 2, Box L5.02.02, 1348 Louvain-la-Neuve, Belgium

[2] Bio-and Soft Matter (BSMA), Institute of Condensed Matter and Nanosciences (IMCN), Université catholique de Louvain (UCL), Croix du Sud 1, Box L7.04.02, 1348 Louvain-la-Neuve, Belgium

polymer production often limits its utilization. However, despite the structural drawbacks, lignin seems to be a prospective candidate for being a component for value-added products in various applications. Recently, an important potential specific to lignin is the production of greener carbon fiber using lignin blended with bio or oil-based polymers [7–12]. This enthusiasm is confirmed by various scientific and technological researches devoted to the synthesis and the characterization of lignin-containing polymers [13–19]. However, raw lignin's incorporation is hindered by its extensive crosslinking and strong intermolecular interactions, therefore making it rarely miscible or finely dispersible with most synthetic polymers leading to negative effects on the mechanical properties [20, 21]. In order to counteract these drawbacks, chemical derivatization of lignin is necessary. Nevertheless, these treatments usually lead to the loss of the environmental and economic advantages of using such raw bio-based resource [22–24].

For practical and ecological reasons as well as for low processing cost, polymers are usually mixed by melt-blending in an extruder. By this way, direct incorporation of raw lignin into bio-based polymer materials like poly(hydroxybutyrate) (PHB), poly(lactid acid) (PLA) have been reported [12, 17, 25, 26]. Blends of lignin and PA11 have been examined only once by Nitz et al. [27] A kraft and two sulfite lignins were studied. The resulted materials were stiff and brittle. They reported that the poor dispersion of lignin particles may have a positive effect on the Young's modulus and the yield stress and a negative one on the elongation at break and the notched impact strength. This behavior originates from the difficulty to prepare miscible blends due to the low entropic benefit of mixing and to its endothermic feature related to a significant absence of intermolecular interactions resulting into phase-separated systems. Therefore, in most cases, some attractive intermolecular interactions between the constituent components must be established to reach miscibility or good compatibility. Miscible blends of lignin up to 40 wt% were for instance observed only in bio-based PHB [25]. Specific hydrogen bonding interactions between the reactive functional groups in lignin with the carbonyl groups of PHB have been brought up by Infrared analysis.

In addition, it is important to note that the presence of filler in the polymer melt largely influences the crystallization behavior and consequently the properties of the resulting product. It is worthwhile noting that to the best of our knowledge, no information is found in the literature about the crystallization behavior under the supercooling rates as a function of the solidification history of PA11 in presence of lignin. This will be specifically examined in this work. Indeed, regarding the structural aspects, PA11 is a polymorphic polymer that exhibits at least five crystal forms: the triclinic α-form, the monoclinic β-form and three hexagonal or pseudo-hexagonal phases (γ, δ and δ'-forms) with different crystal lattices. These phases are largely dependent on thermal history, processing conditions and the presence of fillers [28–31].

The main goal of this paper is to demonstrate the possible use of a commercially produced raw soda lignin powder as a filler for PA11 matrix over the entire concentration range. The incorporation of this renewable material from biomass in PA11 is inspected by an array of characterization tools: Optical and Transmission Electron Microscopy (OM, TEM respectively), Dynamic Mechanical Analysis (DMA), Differential Scanning Calorimetry (DSC), Fast Scanning Chip Calorimetry (FSC) and mechanical testing. Also the effect of the presence of lignin on the morphology and on the properties of the resulting materials is investigated.

Materials and Methods

Materials

The blends were carried out with a commercial soda pulp lignin from agricultural residues (Protobind 1000 by ALM India Pvt. Ltd. Chandigarh 160009, India; $M_n = 65{,}000$ g mol^{-1}, $T_g = 102$ °C, particles size between 20 and 200 µm). Lignin was used as received and was not dried before extrusion. The matrix used was an extrusion grade polyamide 11 having $M_n = 12$ kDa and $M_w = 25$ kDa and manufactured by *Arkema* (France) under the trade name *Rilsan*. Before extrusion PA11 pellets were dried in a vacuum oven at 80 °C for 12 h.

Composite Preparation

Six PA11/lignin blends covering the whole composition range (Table 1) were compounded, using a co-rotating twin-screw extruder Krupp WP ZSK25, with a screw length of 1000 mm and a L/D ratio equal to 40. The extrusion process was conducted at 200 °C with a screw speed of 300 rpm. PA11 and lignin were first pre-mixed together and then introduced in the melting zone using a throughput of 7 kg/h. The residence time in the extruder was around 1.5 min. Finally,

Table 1 Composition of PA11-Lignin blends

Sample	PA11 (wt%)	Lignin (wt%)
PA11-L0	100	0
PA11-L12.5	87.5	12.5
PA11-L25	75	25
PA11-L50	50	50
PA11-L75	25	75
PA11-L87.5	12.5	87.5

extruded samples were immediately quenched at room temperature and pelletized.

Blend pellets were then injection-molded using a Krauss-Maffei type KM 80−160E injection-molding machine in standard dog-bone specimens (ASTM 527) for tensile tests. The barrel temperatures ranged within 180–200 °C and the mold temperature was kept at 25 °C. Before injection, pelletized samples were dried in a vacuum oven at 25 °C for 2 weeks and at 60 °C during 12 h just before the injection-molding.

Characterization Techniques

Structural Characterization

Optical Microscopy The images illustrating the dispersion of the lignin were obtained by means of a binocular optical microscope Ceti Staddy T equipped with a numerical camera Nikon COOLPIX 4500. Examined area of the produced composites was prepared from press molded at 190 °C during 5 s. Micrographs of the samples were taken under magnitude of 60 to provide an actual visual aspect of the samples.

Transmission Electron Microscopy (TEM) A transmission electron microscope LEO 922 (Zeiss) with a 200 kV acceleration voltage was used to examine the dispersion state of lignin in the polyamide matrix. The specimens for TEM analysis were cut from bulk compounds and from the dog-bone specimens at room temperature using a Reichert Microtome. Ultrathin sections of approximately 90 nm thickness were cut using a cryodiamond knife with a cut angle of 35° (Diatome, Switzerland) and collected on 400 mesh copper grids. X-ray Spectrometry coupled with TEM (TEM-EDX) has been used to determine the chemical composition of the samples.

Thermal and Mechanical Characterization

Differential Scanning Calorimetry (DSC) DSC analyses were performed on a DSC 821e (Mettler Toledo, Switzerland). Lignin samples and blend samples of around 10 mg were subjected to a first heating ramp from 25 to 200 °C followed by a cooling ramp from 200 to 25 °C and a second heating ramp from 20 to 220 °C. The heating/cooling rate of each segment was 10 °C/min. The role of the first heating run is usually to erase the thermal history of the sample.

Dynamic Mechanical Analysis (DMA) DMA measurements were carried out using a DMA/SDTA861 (Mettler Toledo, Switzerland) in supported mode in order to highlight the lignin thermal transitions. Supported DMA was achieved on samples powder sandwiched between rigid copper foils (of dimension $8\times0.3\times70$ mm^3) and the whole was packed by an aluminum sheet to avoid any sample loss. This technique has already been used to assess thermal properties of coatings and nanocoatings by Carlier et al. and demonstrated that the response from the less stiff material is mainly recorded and strongly amplified [32]. Like in Carlier's work, lignin system was subjected to a dual cantilever deformation in order to favor the shear strain of the lignin. The maximum force was 1.5 N and the maximum displacement was 10 µm. The analyses were performed at a constant frequency of 1 Hz from −50 to 200 °C with a heating rate of 3°C/min. A first heating was performed in order to homogenize the different samples.

Fast Scanning Chip Calorimetry (FSC) FSC measurements were performed on a Flash-DSC1 (Mettler Toledo, Switzerland) equipped with an intracooler, which enables a minimum temperature of about −90 °C. The investigated temperature range was set from −20 to 220 °C. The influence on the cooling rate was first investigated in order to determine the critical cooling rate allowing to produce a fully amorphous PA11. Moreover, the kinetics of crystallization on isothermal steps (2 s) from 160 to 40 °C with an incremental step of 10 °C was studied as well. The applied cooling and heating rates were −1000 °C/s and 1000 °C/s, respectively. Samples with a thickness of about 10 µm and an approximate mass of between 20 and 100 ng were deposited on a MultiSTAR UFS 1 chip sensor using a microscope. The glass transition temperatures (Tg) as well as the melting peaks of the neat and modified PA11 samples were defined as the midpoint and the maximum peak of the FSC curves.

Mechanical Testing

Tensile tests were carried out at room temperature using a universal tensile machine (Zwick Roell RetroLine) equipped with a 50 kN load cell. All injection-molded specimens had a dog-bone shape according to the standard ISO 527-3 type V, with an average cross section of 5.7×2 mm^2 at the gauge length region. Strain was accurately determined using an extensometer and a crosshead speed of 1 mm/min. The Young's modulus was calculated from the slope of the stress–strain curve in the elastic regime (between 0.05 and 0.02% strains). The tensile yield strength and the elongation at break were measured at a loading rate of 50 mm/min. Property values reported in this work represent an average of three replicates for each sample.

Results and Discussion

Morphological Characterization

Interestingly, while processing, all compositions exhibited a plasticizing effect which allowed achieving high

concentrations of lignin in PA11. This plasticizing effect indicates probable inter-chain interactions upon changing blend composition and has been already described for Protobind 1000 lignin/PA6 blends, for kraft and organosolv lignin/PEO blends [33–35]. The cooled strand could be stretched by hand like pristine matrix at 12.5 and 25 wt% of lignin, whereas above 50 wt%, the extruded strand is increasingly brittle.

The efficiency of the lignin in reinforcing the polymer matrix is primarily determined by the degree of its dispersion into the matrix. As the extruded samples take a sustained brown tint due to the presence of lignin, the degree of dispersion of lignin cannot be easily distinguishable by the naked eye. Therefore, Optical microscopy (OM) observations were carried on hot press molded films of 0.1 mm in order to have a fine approach of the dispersion state in the different composites. Figure 1 shows the optical images of PA11-L12.5, 25, 50, 75 and 87.5. The OM micrographs were carried out on a large number of samples and the micrographs reported on Fig. 1 are representative of the observed morphology. The grey area due to the presence of lignin can be guessed at 50 wt%, it is confirmed at higher lignin concentration. No aggregates of lignin are visible in the two first concentrations explaining the possibility of the hand stretching described above and conversely the decrease of the mechanical strength of the strand for the high lignin's concentration. At these high concentrations, the presence of a few cellulose fibers is even observed since lignin is used as received. This kind of impurity is already identified for Protobind P1000 [35].

In order to confirm the achievement of the dispersion of lignin in the matrix, TEM observations were carried out. Figure 2 reports characteristic micrographs at 16,000 magnification obtained for extruded PA11 with the first three concentrations of lignin. Above 50 wt% of lignin, no ultrathin sections could be obtained due to their weakness. At this scale and confronted to the case of pristine PA11, no trace of aggregates were visible for the first concentration of lignin. However, the two following concentrations (25 and 50 wt% of lignin), both show well-dispersed aggregates. Their diameters are inferior to 200 nm and 400 nm, respectively. The grey area corresponds to the PA11 matrix and the darker particles are attributed to lignin. The black sub inclusions particles were identified by EDX-TEM and were attributed to silica particles already described (Fig. 3) [36]. They are localized within the lignin's particles. Their high dispersion for the lower concentration of lignin suggests miscibility of both components. The injected specimens yield the same morphological images (not shown here).

Thermo-Mechanical Properties

In order to investigate more accurately the miscibility of PA11/lignin blends, the glass transition temperatures (T_g) have been obtained using DMA measurements. DMA is a very sensitive technique and provides a valuable insight into the relationships between morphology, components interactions and mechanical properties of composite materials. T_g is usually defined as the peak in the loss modulus (E") versus temperature curves. Figure 4 shows the temperature dependence in the glassy region of the loss factor (Tan δ) of neat PA11 and lignin in comparison with their blends. Corresponding T_g values are listed in Table 2. Except for PA11-L75 and 87.5, all samples exhibit a single and broad peak, related to the glass transition temperature (T_g), which shifts to higher temperatures with increasing lignin content. This glass transition, broader than those of the parent components, is usually observed in miscible polymer blends. This behavior is caused by the intrinsic difference between the local chain segment mobility of PA11 and lignin components. Moreover, adding lignin increases the T_g from 67 °C for neat PA11 to 91 °C for PA11-L75. The fact that a single T_g was observed in the blends indicates the existence of a single-phase system with homogeneous miscibility at a dimensional scale of 5 and 15 nm and a high specific interaction system [37–39]. This observation confirms the morphological investigations by TEM indicating that PA11 and lignin are homogenous and miscible. In the case of very high content of lignin as it is the case for the blend PA11-L75, two T_gs have been measured between those of the parent polymers, suggesting that the degree of miscibility is restricted. This behavior could be also ascribed to the sample's saturation with lignin [25].

The fact that the incorporation of lignin affects significantly the glass transition temperature of the blend, means that the overall chain mobility is very sensitive to the presence of lignin. The latter increases the contribution of the viscous part to the dynamic response and decreases chain entanglement in the rubbery plateau region, which in turn decreases the thermal stability of the composites at higher temperature. The same phenomenon has been observed in literature [35].

DSC was performed to study the effect of lignin content on the thermal behavior of PA11-lignin composites, particularly, the crystallization temperature (T_c) and the melting point (Tm). T_gs were measured only for PA11 and lignin and are about 47 and 140 °C, respectively. Those are lower than the ones determined by DMA because of the difference in solicitations and equipment. The one measured by DSC is a thermal T_g and does not exactly correspond to the dynamical T_g determined by DMA. These differences are well documented in literature [40, 41]. The intrinsic broadened transition of lignin hinders the clear observation of the blends'

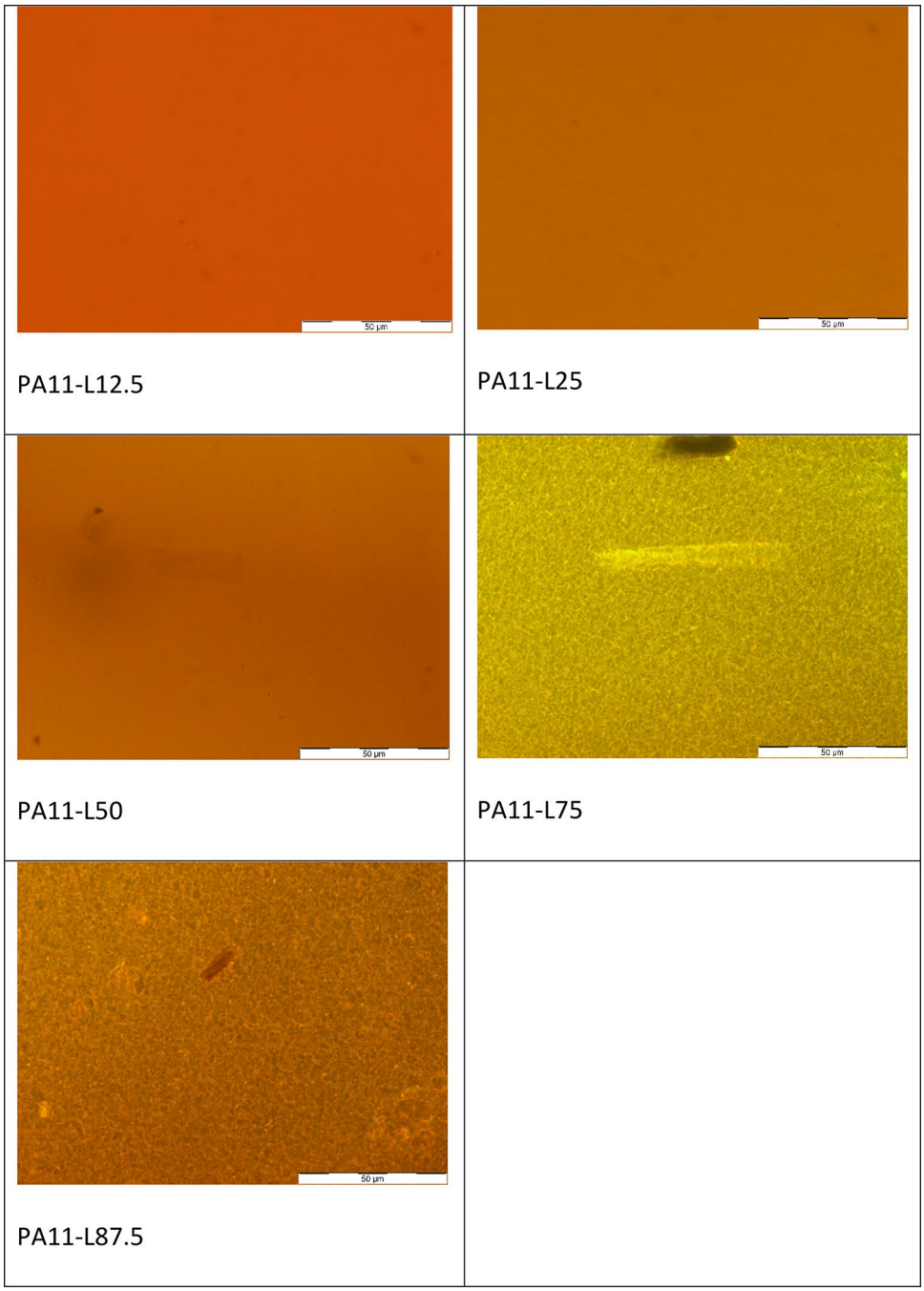

Fig. 1 Optical microscopy observations of PA11/Lignin films

T_g due to its highly amorphous nature and to its complex hydrogen bonding interactions, which can induce significant enthalpy relaxation [35, 42]. Figure 5a, b depict the DSC thermograms recorded during cooling from the melt and subsequent heating, respectively for PA11-L0, lignin and the blends. The values of T_c and T_m measured from these measurements are reported in Table 3.

As observed on Fig. 5a and in Table 3, the T_cs shift by flattening to lower temperatures as lignin content increases even to disappear with high content of lignin (87.5 wt%). This evolution shows that the crystallization process of PA11 is delayed or even prevented at 87.5 wt% of lignin. This behavior is an indication of intermolecular interactions between different species through hydrogen bonds, leading to a significant evolution of the supermolecular structure mainly in terms of the PA11 crystal dimensions which hinders the formation of large crystalline structures. A similar effect has already been observed for the blends PEO/lignin and PA6/lignin [33–35, 42].

PA11 shows an endotherm peak with a bimodal shape around 150–190 °C (Fig. 5b; Table 3). This phenomenon has been ascribed to a melting-recrystallization process of

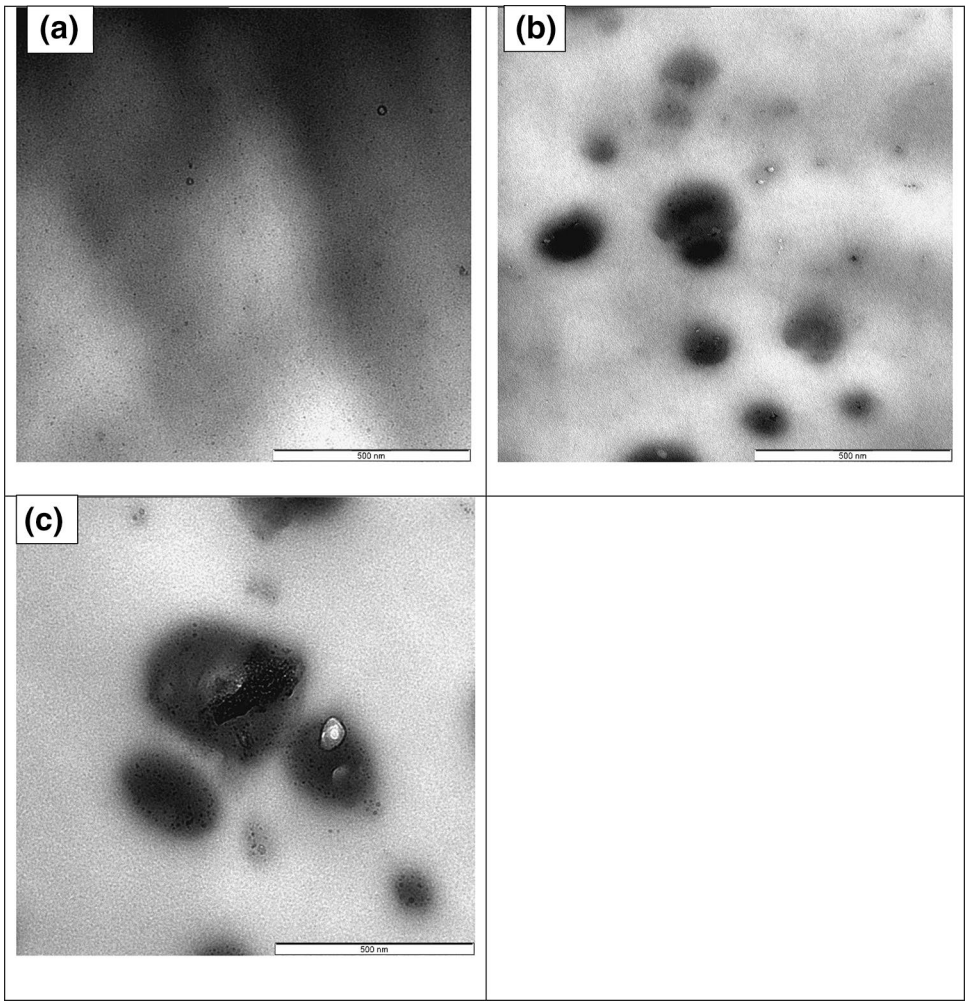

Fig. 2 TEM micrographs of: **a** PA11-L12.5, **b** PA11-L25 and **c** PA11-L50

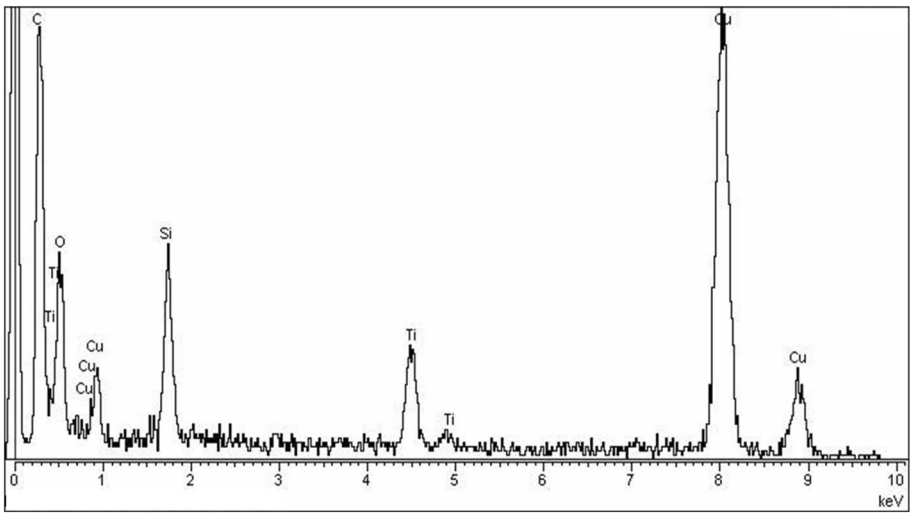

Fig. 3 EDX-TEM characterization of the black sub inclusions particles inside lignin particles for the PA11-L25 blend

defective crystallites formed due to processing conditions leading either to the formation of two forms of crystals or to one type of crystal exhibiting different degrees of perfection [31, 43, 44]. With addition of lignin up to 75 wt%, the bimodality is maintained but associated to a decrease of crystallinity level (χ_c) and T_m due to thermodynamical interactions. χ_c varies from 27% for PA11-L0 to 0.7% for PA11-L87.5 (Table 3). Particularly, the latter shows a same

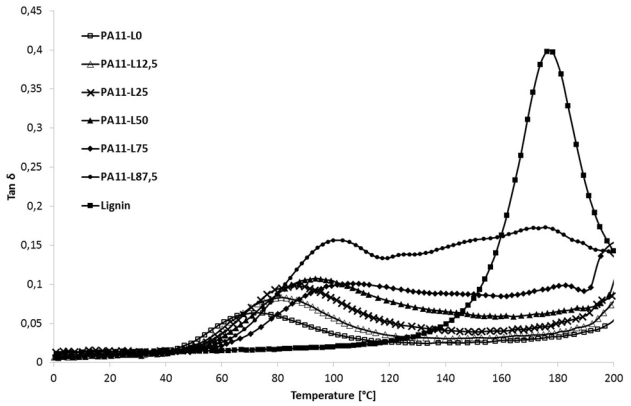

Fig. 4 Phase angle (Tan δ) of neat lignin and of lignin/PA11 blends

Table 2 Glass transition temperatures (Tg) of references and lignin/PA11 blends measured from the loss modulus (E")

Samples	Tg (°C)
PA11-L0	67
PA11-L12,5	75
PA11-L25	77
PA11-L50	80
PA11-L75	91
PA11-L87.5	90 133
Lignin	162

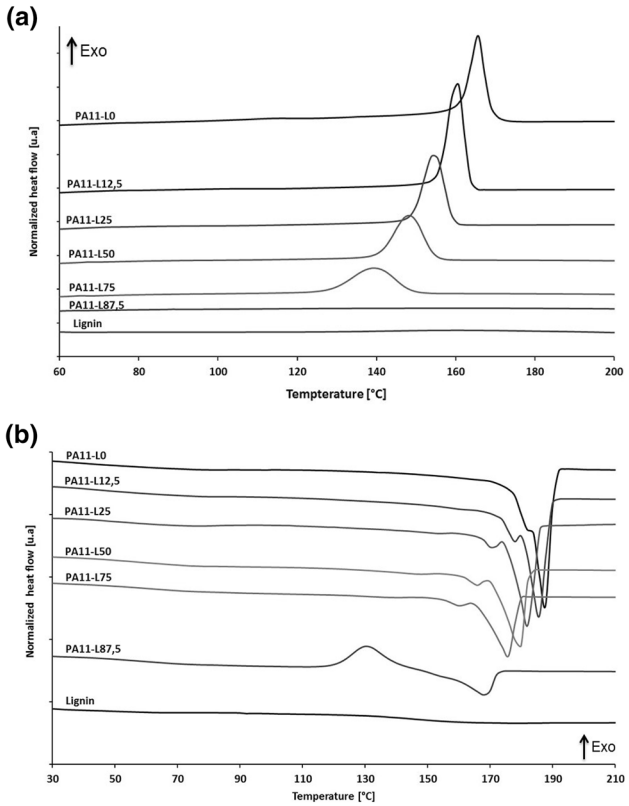

Fig. 5 DSC thermograms of PA11/lignin composites recorded upon **a** cooling; and **b** second heating

amplitude in exothermic cold crystallization peak preceding the endotherm peak. The weak enthalpy close to zero indicates a retardant/absence of PA11 crystallization due to the hindrance of the motion of PA11 chains in the presence of lignin particles [45]. The effect of the heating rate for this last concentration of lignin (Fig. 6), invariably shows, at a heating of 50 °C/min, the presence of a cold crystallization associated to a low enthalpy peak area, which highlights the influence of lignin particles on the PA11 crystallization process.

Therefore, these results indicate that up to 75 wt% of lignin, specific interactions exist between lignin and PA11, which influence the crystallization process of PA11. The effect of the cooling rate on the crystallization process of PA11 will be analyzed by FSC in the following section in order to study the PA11 crystallization kinetics in presence of lignin.

The influence of the cooling rates on the crystallization of PA11 was first investigated in order to determine the critical cooling rate allowing to produce a fully amorphous PA11. Figure 7 shows the evolution of the apparent heat capacity corresponding to a heat flow normalized to the cooling rate of neat PA11, measured at different cooling rates from 10 to 1000 °C/s. A cooling rate lower than 10 °C/s (see DSC results) leads to a single crystallization

Table 3 DSC measurements of PA11 and its blends

Sample	T_c (°C)	T_m (°C)	χ_c (%)
PA11-L0	166	186	27
PA11-L12.5	160	182	23
PA11-L25	154	179	14
PA11-L50	148	177	8
PA11-L75	139	173	3
PA11-L87.5	–	168	0.7

peak (the crystallization peak temperature is about 166 °C). For cooling rates lower than 500°C/s, two crystallization peaks are actually visible during crystallization from the melt and the crystallization peak temperature range is between 140 and 40 °C. The second crystallization peak still remains at low temperature while the first one, visible at higher temperature, totally disappeared at cooling rates equivalent to 300 and 500 °C/s. Nevertheless, a cooling rate slightly above 500 °C/s and higher does no longer lead to crystallization of PA11 and hence, defines this cooling rate as the critical cooling rate for PA11 amorphization. In this study, the amorphization rate was fixed at 1000 °C/s.

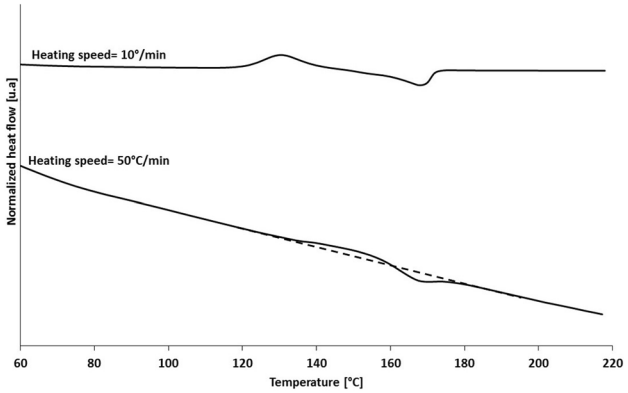

Fig. 6 Effect of the heating rate on PA11-L87.5 crystallization process

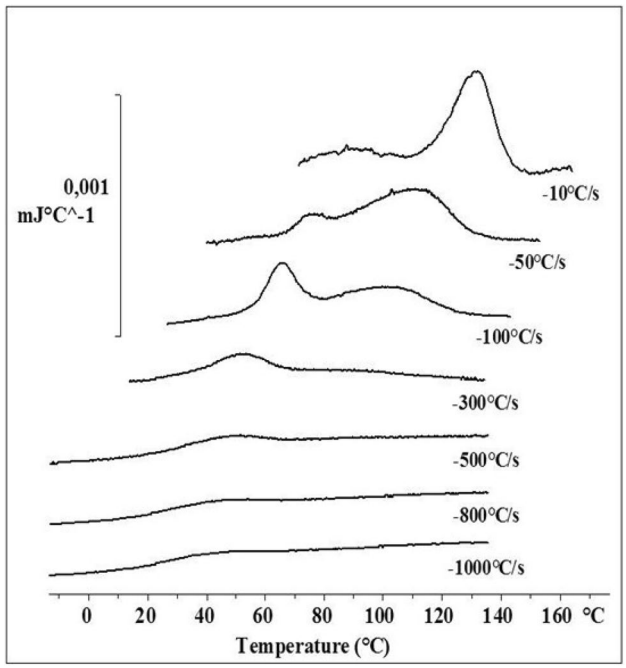

Fig. 7 Apparent heat capacity versus temperature of neat PA11 (PA11-L0)

Figure 8 graphically shows the maximum temperatures of the neat PA11 crystallization peaks as a function of the cooling rate from 0.16 to 1000 °C/s. Data were obtained by DSC and FSC. PA11 crystallization upon supercooling rates has been studied by Mollova et al. [29] Equivalent behaviors have been obtained and the same conclusions could be drawn. Cooling rates lower than 100 °C/s lead to crystallization and formation of δ-crystals at relatively high temperature while for faster cooling (up to 500 °C/s), δ'-mesophase is formed at relatively low temperature. For cooling rates between 10 and 100 °C/s, both phases seem to be present [29].

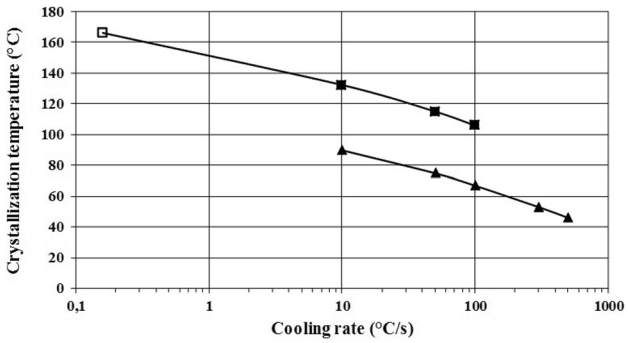

Fig. 8 Crystallization peak versus cooling rate of neat PA11

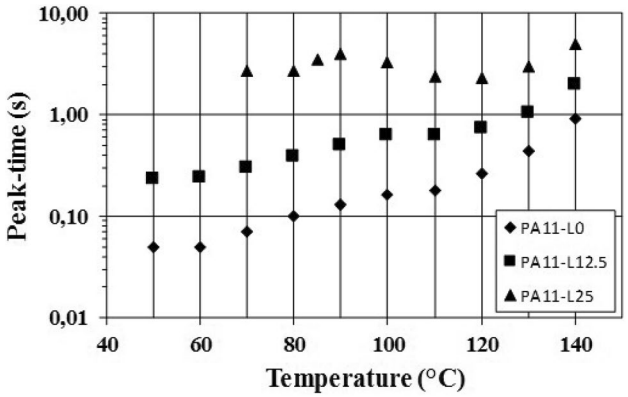

Fig. 9 Peak time versus crystallization temperature for isothermal temperature of PA11-L0 and PA11-L12.5 and 25

Moreover, the kinetic of crystallization on isothermal steps was also studied. The sample in its molten state is rapidly cooled down at 1000 °C/s (to avoid any crystallization) to a chosen temperature (varying between T_m and T_g) and held for a specific time (2 s), cooled down at − 20 °C at the same cooling rate and then reheated to 220 °C at 1000 °C/s. The amount of the crystalline phase allowed forming during the isothermal step can be easily observed and calculated from the subsequent heating curves. Measurements of the isothermal crystallization of PA11-L0 and blends of PA11-L12.5 and 25 were performed in a temperature range from 160 to 40 °C. For higher lignin content (50, 75 and 87.5 wt%), no crystallization processes occur in this applied FSC cooling rates range. The peak time of the isothermal crystallization peaks as a function of the crystallization temperature are shown in Fig. 9. Both neat PA11 and PA11 blends reveal bimodal crystallization behaviors with a high temperature and a low temperature regime (below 100 °C) corresponding to the formations of δ-crystal and δ'-mesophase explained with a change of nucleation mechanism from heterogeneous to homogeneous nucleation, respectively, as already described in literature [29]. Two

Table 4 Mechanical properties of PA11/lignin blends

Samples	Young's modulus [MPa]	Yield stress [MPa]	Elongation at break [%]
PA11-L0	990 ± 22	37 ± 1	195 ± 31
PA6-L12.5	1331 ± 366	39 ± 1	172 ± 7
PA6-L25	1663 ± 90	53 ± 2	9 ± 2

distinct minima of peak time of crystallization are observed at approximately 60 and 120 °C. Although the bimodal crystallization shapes are relatively similar, the presence of lignin in PA11 seems to significantly decelerate the kinetics of crystallization, proportionally to the lignin concentration. A delayed crystallization peak (obtained for a cooling rate of 10°C/min) with increasing lignin content was also observed by DSC and is in good agreement with FSC results.

Mechanical Properties

The effect of lignin addition on the mechanical properties of PA11 beyond 25 wt% of lignin because of the samples weakness has been studied based on uniaxial stretching at room temperature.

Table 4 summarizes the tensile properties of PA11-L0 and its blends. Not shown, PA11-L0 displays a typical tensile behavior of semi-crystalline polymers. However, regarding the blends, the behavior depends on lignin content. PA11-L12.5 blend exhibits a very similar behavior as PA11-L0. The elongation at break is slightly lower but remains very close to the one of PA11. This very small decrease in ductility can be ascribed to both lignin plasticization and miscible blending between PA11 and lignin. Similar trends have been observed for miscible blends of PA6 and lignin, for a partially miscible blend of Polyvinylidene fluoride and Polytetramethylene adipate or for a compatibilized composite of Polyethylene and modified lignin via an esterified route [24, 46].

In the case of PA11-L25, the lignin's addition implies an increase of both the yield stress and the Young's modulus. In opposition, a sharp decrease of the strain at break is observed. This behavior is currently encountered when nanoparticles are added into a polymer matrix. An explanation can be found in the decrease of the molecular mobility induced by the presence of lignin particles that involves a lack of deformability of the polymer within the interphase close to the particle. Indeed, for this concentration significant well-dispersed aggregates (see TEM pictures) are present. They are probably responsible for the material's embrittlement, acting as stress concentrations points. The presence of impurities as silica could also explain this behavior (see EDX-TEM results).

Conclusions

100% bio-composite has been prepared based on PA11 and technical lignin via twin screw extrusion process and was found to be miscible as deduced from structural and thermal investigations showing homogeneous blends. PA11/Lignin miscibility has been observed for lignin amount up to 25 wt%. The T_g is shifted to high temperature upon blending indicating strong intermolecular interactions. Also, PA11 blends reveal a bimodal crystallization behavior through the investigated temperature range. Moreover, the presence of lignin significantly delays the kinetics of PA11 crystallization. Regarding the mechanical properties, lignin addition leads to an increase of both the yield stress and the Young's modulus. However, concerning the strain at break the bio-composite behaves differently depending on lignin concentration. For a lignin content inferior to 12.5 wt%, the elongation at break is very close to the virgin PA11 one due to lignin plasticization effect and its matrix' miscibility. On the contrary, above 12.5 wt% of lignin, the sharp decrease of the strain at break is assigned to the presence of significant aggregates/contaminations.

Acknowledgements The authors acknowledge the support from Walloon Region (DEXPLIMAR Project No. 6758).

References

1. Niaounakis M (2015) Biopolymers: applications and trends. Elsevier, New York, 978-0-323-35399-1
2. Zierdt P, Theumer T, Kulkarni G, Däumlich V, Klehm J, Hirsch U, Weber A (2015) Sustain Mater Technol 6:6
3. Brebu M, Vasile C (2010) Cell Chem Technol 44:353
4. Delmas M (2008) Chem Eng Technol 31:792
5. Kamm B, Kamm M (2004) Appl Microbiol Biotechnol 64:137
6. Ragauskas AJ, Williams CK, Davison BH, Britovsek G, Cairney J, Eckert CA, Frederick WJ, Hallett JP, Leak DJ, Liotta CL, Mielenz JR, Murphy R, Templer R, Tschaplinski T (2006) Science 311:484
7. Brodin I, Ernstsson M, Gellerstedt G, Sjöholm E (2012) Holzforschung 66:141
8. Kadla JF, Kubo S (2003) Macromolecules 36:7803
9. Kadla JF, Kubo S, Venditti RA, Gilbert RD, Compere AL, CW Griffith (2002) Carbon 40:2913
10. Kubo S, Kadla JF (2005) J Polym Environ 13:97
11. Ramasubramanian G (2013) Graduate Theses and Dissertations. Paper 13438
12. Thunga M, Chen K, Grewell D, Kessler MR (2014) Carbon 68:159
13. Canetti M, Bertini F, De Chirico A, Audisio G (2006) Polym Degrad Stab 91:494
14. Dawson BSW, Singh AP, Kroese HW, Schwitzer MA, Gallagher S, Riddiough SJ, Wu SHJ (2008) J Coat Technol Res 5:193
15. Ismail T, Abu Hassan H, Hirose S, Taguchi Y, Hatakeyama T, Hatakeyama H (2010) Polym Int 59:181
16. Košíková B, Gregorová A, Osvald A, Krajcŏvicŏva J (2007) J Appl Polym Sci 103:1226
17. Li J, He Y, Inoue Y (2003) Polym Int 52:949

18. Pouteau C, Dole P, Cathala B, Averous L, Boquillon N (2003) Polym Degrad Stab 81:9
19. Saito T, Brown RH, Hunt MA, Pickel DL, Pickel JM, Messman JM, Baker FS, Keller MA, Naskar K (2012) Green Chem 14:3295
20. Alexy P, Košíková B, Podstránska G (2000) Polymer 41:4901
21. Kubo S, Kadla JF (2005) Biomacromolecules 6:2815
22. Laurichesse S, Avérous L (2014) Progress in Polym Sci 39:1266
23. Sadeghifar H, Cui C, Argyropoulos DS (2012) Ind Eng Chem Res 51:16713
24. Sailaja RRN, Deepthi MV (2010) Mater Des 31:4369
25. Mousavioun P, Doherty WOS, George G (2010) Ind Crops Prod 32:656
26. Rahman MA, De Santis D, Spagnoli G, Ramorino G, Penco M, Phuong VT, Lazzeri A (2013) J Appl Polym Sci https://doi.org/10.1002/APP.38705
27. Nitz H, Semke H, Mülhaupt R (2001) Macromol Mater Eng 286:737
28. Kolesov I, Androsh R, Mileva D, Lebek W, Benhamida A, Kaci M, Focke W (2013) Colloid Polym Sci 291:2541
29. Mollova A, Androsch R, Mileva D, Schick C, Benhamida A (2013) Macromolecules 46:828
30. Stoclet G, Sclavons M, Devaux J (2013) J Appl Polym Sci https://doi.org/10.1002/APP.38053
31. Zhang G, Li Y, Yan D (2004) J Polym Sci Part B Polym Phys 42:253
32. Carlier V, Sclavons M, Legras R (2001) Polymer 42:5327
33. Kubo S, Kadla JF (2005) J Appl Polym Sci 98:1437
34. Kubo S, Kadla JF (2004) Macromolecules 37:6904
35. Sallem-Idrissi N, Vanderghem C, Pacary T, Richel A, Debecker DP, Devaux J, Sclavons M (2016) J Appl Polym Sci https://doi.org/10.1002/APP.42963
36. Sahoo S, Seydibeyoglu M, Mohanty AK, Misra M (2011) Biomass Bioenergy 35:4230
37. Mishra SB, Mishra AK, Kaushik NK, Khan MA (2007) J Mater Process Technol 183:273
38. Paul DR, Bucknall CB (2000) Polymer blends: formulation and performance, 1. John Wiley & Sons, Hoboken, pp 539–579
39. Woo EM, Wu MN (1996) Polymer 37:907
40. Schawe JEK (1998) J Polym Sc Part B Polym Phys 36:2165
41. Schawe JEK (2002) Elastomers Collected applications thermal analysis, 1. Mettler Toledo, Columbus, pp 35–46
42. Bittencourt PRS, Fernandes DM, Silva MF, Lima MK, Hechenleitner AAW, Pineda EAG (2010) Waste Biomass Valor 1:323
43. Stoclet G, Seguela R, Lefebvre J-M (2011) Polymer 52:1417
44. Zhang Q, Yu M, Fu Q (2004) Polym Int 53:1941
45. Wu M, Yang G, Wang M, Wang W, Zhang W-D, Feng J, Liu T (2008) Mater Chem Phys 109:547
46. Reckinger C, Rault J (1986) Revue Phys Appl 21:11